

# Surface Model Based Modeling and Simulation of Filling Process in Gas-Assisted Injection Molding

Jianhui Li

Lei Chen

Huamin Zhou<sup>1</sup>

e-mail: hmzhou@hust.edu.cn

Dequn Li

State Key Laboratory of Mold and Die Technology,  
Huazhong University of Science and Technology,  
1037 Luoyu Road,  
Wuhan,  
Hubei 430074, China

*Present gas-assisted injection molding simulations are all based on either a midplane model or a 3D model, in which second modeling is unavoidable for a midplane model, and a 3D simulation needs a full-scale three-dimensional discretization of parts leading to unsustainable computing time and unstable numerical analysis. In this paper, surface model based modeling and numerical simulation of gas-assisted injection molding are proposed. By taking the influence of gas penetration on melt flow as boundary conditions of the melt-filling region, a hybrid control-volume finite element/finite-difference method (CV/FEM/FDM) similar to conventional injection molding simulation is employed. The gas penetration interface within the gas channel is solved by applying the matching asymptotic expansion method, which educes an analytical model of the gas penetration thickness ratio. A technology of generating gas-channel mesh semiautomatically is put forward, which combines selecting the path of gas channel manually and calculating the parameters of gas nodes automatically. The second modeling is thus avoided. The proposed model and simulation are verified by comparing with the experiment.*

[DOI: 10.1115/1.3063653]

*Keywords:* surface model, GAIM, numerical simulation, matching asymptotic expansion method

## 1 Introduction

Gas-assisted injection molding (GAIM) has become one of the most popular multicomponent injection molding processes in recent years [1]. Once the mold cavity is partially filled with molten polymers, gas is injected into the mold either at the nozzle or from within the cavity. The gas cores out the center of the thicker sections of the molded part and pushes the molten polymer further into the mold until it is fully filled, thus yielding a product with a polymer skin and a hollow core. The gas is then used to transmit the packing pressure to compensate for polymer shrinkage and is vented just prior to demolding [2,3].

This process can substantially reduce operating expenses as well as improve product quality through reduction in residual stress. Therefore, it has come into practice and has been spread extensively. Despite such advantages, the mold design and process control become more critical and difficult since additional process parameters are involved, including the melt short shot size, gas pressure, delay time of gas injection, and gas injection duration. Product, tool, and process designs for gas-assisted injection molding are quite complicated, and experiences with conventional injection molding are no longer sufficient for this process. The computer simulation for GAIM is, therefore, expected to be an important and a required tool in part design and process evaluation.

The injected gas typically penetrates along the path of least flow resistance [4]. In order to lead the gas to the locations where sink marks most likely occur, GAIM products are generally designed containing gas channels. Among them, there are essentially two types: parts with solid thin walls reinforced with hollow ribs and those where the gas core forms a hollow interior extending throughout all or most of the part [5]. Four regions can be iden-

tified during gas-assisted injection molding (as shown in Fig. 1). These four regions are confined by the melt and gas fronts. The melt front in this process is identical to that in conventional injection molding. Pressure and temperature in the gas penetration region are considered uniform everywhere, and the influence of gas penetration on melt flow is reflected on gas penetration interface [1].

During the past decades, many GAIM simulation softwares, such as MOLDFLOW, MOLDEX3D, TIMON, etc., have been developed, which are all based on either a midplane model or a 3D model. Second modeling is inevitable for the midplane model and its corresponding gas channel. With regard to the full 3D simulation, it needs a full-scale three-dimensional discretization of thin parts, which leads to unsustainable computing time and instability of calculation. The GAIM simulation, therefore, is not applied widely in practice.

A method of GAIM simulation based on the surface model is introduced in this paper. The surface model, comprised of a certain amount of triangle elements generated by the Delaunay triangulation method based on a stereolithography (STL) model, has been applied widely in the computer aided engineering (CAE) software, and the numerical solution of nonisothermal non-Newtonian fluid based on a surface model has been well established [6,7]. Additional problems of GAIM filling simulation based on a surface model are gas-channel mesh generation and the numerical solution of gas penetration interface.

As for the gas-channel mesh generation, there still lacks a reasonable approach. Since the pressure of gas is identical in all directions, the cross section of a gas channel is usually circular [3]. Therefore, in this paper, the technology of generating a cylindrical gas-channel mesh semiautomatically was conducted by combining selecting the path of gas channel manually and calculating the parameter of a gas node automatically using gradual approximation method. The troublesome second modeling could be avoided in this way.

As for the numerical solution of the gas penetration interface, the mechanism is similar to that of the displacement of a more viscous fluid in a tube by a less viscous fluid. The residual wall

<sup>1</sup>Corresponding author.

Contributed by the Manufacturing Engineering Division of ASME for publication in the JOURNAL OF MANUFACTURING SCIENCE AND ENGINEERING. Manuscript received December 17, 2007; final manuscript received December 7, 2008; published online January 13, 2009. Review conducted by Jyhwen Wang.

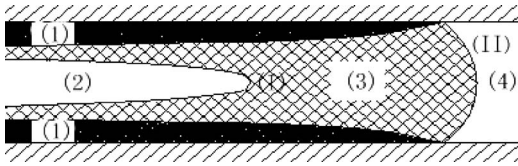


**Fig. 1 Schematic notation for flow regions and their interface in gas-assisted injection molding: (1) the solid frozen layer, (2) the penetration gas, (3) the deforming viscous melt, (4) the unfilled cavity, (I) the gas front, and (II) the melt front**

thickness is determined by the capillary number  $Ca = \eta U / \lambda$ , where  $U$  is the velocity,  $\eta$  is the viscosity of fluid, and  $\lambda$  is the gas–liquid interfacial tension [5]. Many theoretical and experimental studies have been carried out on the physics process. Yang and co-workers [8,9] studied the effect of the gas-channel dimension on gas penetration. Huzyak and Koellin [10] investigated isothermal gas penetration of Newtonian melts in circular tubes by experiments. Polynkin et al. [11] experimented on gas penetration in tubes thoroughly. Ilinca [12] tracked the gas front and melt front using the pseudoconcentration method. Bretherton [13] conducted an analytical approximation of the governing equations for small capillary numbers, using matched asymptotic expansion method. Reinelt and Saffman [14] and Kolb and Cerro [15] obtained numerical solutions in close agreement with the data for Newtonian melts. Zhou [1] extended Bretherton’s solution to higher capillary numbers using the correctional equation. Belblidia et al. [16] investigated dimensionless correlations for predicting the layer thickness formed when gas displaces liquid in a 2D straight cylindrical tube. The study results are helpful in improving existing computer simulations by simplifying the geometry of molded parts and by representing the channels cored out by the gas as equivalent cylindrical tubes. Shen [17] also studied gas penetration phenomenon with 2D gas channel. Chen et al. [18] converted gas channel into equivalent circular pipe and further simplified it into two-node elements using line source methods, which only affects the calculation accuracy very slightly and reduces the computer time by 93%.

A practical method for simulating the filling process of the gas-assisted injection molding with circular channels was developed herein. In Sec. 2, gas penetration thickness was derived by solving the theoretical equations governing the behavior of the gas penetration by employing the matching asymptotic expansion method. In Sec. 3, a technology for generating gas-channel mesh semiautomatically was conducted, which avoided the troublesome second modeling. Based on the derived equations and the gas-channel mesh, numerical solution was implemented. Finally, the predicted result was compared with experimental observation for verification.

## 2 Modeling and Formulation

**2.1 Model of Gas and Melt Flow.** The most important characteristic of GAIM is that the pressure gradient in the gas core region is negligibly small compared with that in an equivalent polymer melt region, which is due to high viscosity ratio of polymer to gas. Consequently, the pressure may be assumed constant through the gas core. In addition, the gas penetration velocity is higher than the velocity of the melt front, so the thermal conductivity can be neglected with respect to the melt. Therefore, the governing equations of the gas region are

$$P = P(t), \quad T = T(t) \quad (1)$$

Like conventional injection molding, melt flow of GAIM is assumed to obey the governing transport equations for incompressible generalized Hele–Shaw flow of inelastic, non-

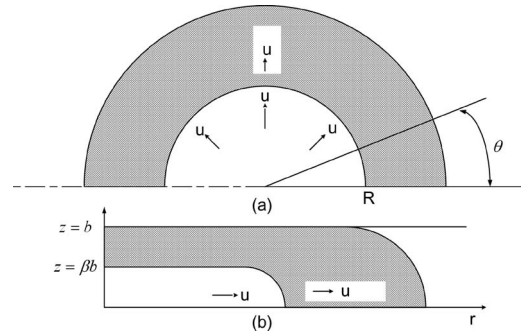


**Fig. 2 Schematic notation for gas penetration in circular gas channel: (a) radial penetration and (b) axial penetration**

Newtonian fluids under nonisothermal conditions. Taking the reasonable simplifications, the governing equations are described as [6] follows:

$$\frac{\partial}{\partial z} \left( \eta \frac{\partial u}{\partial z} \right) - \frac{\partial P}{\partial x} = 0 \quad (2a)$$

$$\frac{\partial}{\partial z} \left( \eta \frac{\partial v}{\partial z} \right) - \frac{\partial P}{\partial y} = 0 \quad (2b)$$

$$\frac{\partial}{\partial x} (b\bar{u}) + \frac{\partial}{\partial y} (b\bar{v}) = 0 \quad (2c)$$

$$\rho C_p \left( \frac{\partial T}{\partial t} + u \frac{\partial T}{\partial x} + v \frac{\partial T}{\partial y} \right) = k \frac{\partial^2 T}{\partial z^2} + \eta \left( \left( \frac{\partial u}{\partial z} \right)^2 + \left( \frac{\partial v}{\partial z} \right)^2 \right) \quad (2d)$$

where  $x$  and  $y$  are planar coordinates in the stream plane and  $z$  is the gapwise coordinate with  $b$  denoting the half-gap thickness, whereas  $u$  and  $v$  are velocity components in the  $x$  and  $y$  directions and  $\bar{u}$  and  $\bar{v}$  are the averaged velocities in the whole-gap thickness in the  $x$  and  $y$  directions. In addition,  $P$ ,  $T$ , and  $t$  are the pressure, temperature, and time, while  $\eta$ ,  $\rho$ ,  $C_p$ , and  $k$  are the viscosity, density, specific heat, and thermal conductivity of the melt, respectively.

## 2.2 Model and Solution of Gas Penetration

**2.2.1 Governing Equations and Boundary Conditions.** As shown in Fig. 2,  $U$  is the gas penetration velocity,  $\beta$  is the penetration thickness ratio, i.e., the ratio of the gas penetration thickness to that of the mold cavity. All parameters keep unchanged along  $\theta$  direction [16].

$$\frac{\partial P}{\partial \theta} = \frac{\partial u}{\partial \theta} = \frac{\partial v}{\partial \theta} = \frac{\partial w}{\partial \theta} = 0 \quad (3)$$

The governing equation can be given as

$$\frac{\partial u}{\partial r} + \frac{u}{r} + \frac{\partial w}{\partial z} = 0 \quad (4a)$$

$$\frac{\partial P}{\partial r} = \eta \left[ \frac{\partial^2 u}{\partial r^2} + \frac{1}{r} \frac{\partial u}{\partial r} + \frac{\partial^2 u}{\partial z^2} - \frac{u}{r^2} \right] \quad (4b)$$

$$\frac{\partial P}{\partial z} = \eta \left[ \frac{\partial^2 w}{\partial r^2} + \frac{1}{r} \frac{\partial w}{\partial r} + \frac{\partial^2 w}{\partial z^2} \right] \quad (4c)$$

At the interface of the gas and melt, it is assumed that the gas and melt are separated completely, as given by

$$(\hat{V}_m - \hat{V}_g) \cdot \vec{n} = 0 \quad (5)$$

where  $\hat{V}_m$  and  $\hat{V}_g$  represent the velocity of the melt and gas at the interface, respectively, and  $\vec{n}$  is the unit vector normal to the in-

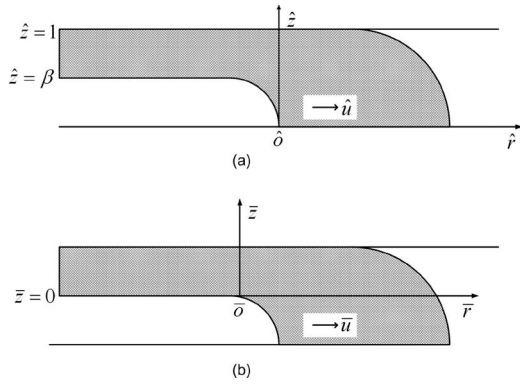


**Fig. 3 Illustration for (a) the outer coordinate system and (b) the inner coordinate system**

terface. In the present coordinate system,  $\vec{n} = (n_r, n_\theta, n_z)$ , in view of  $n_\theta = 0$ , which leads to the continuity Eq. (8a).

By considering the stress balance at the interface, the tangential stress boundary condition is given by

$$\tau_{zz}n_z t_z + \tau_{rz}n_r t_z + \tau_{zr}n_z t_r + \tau_{rr}n_r t_r = 0 \quad (6)$$

The difference in the normal stress on the two sides of the interface is balanced by surface tension and is expressed as

$$\tau_{zz}n_z^2 + 2\tau_{rz}n_r t_z + \tau_{rr}n_r^2 = -P_0 + \lambda \left( \frac{1}{R_1} + \frac{1}{R_2} \right) \quad (7)$$

where  $\tau_{ij}$  is the total stress tensor of the melt, and  $\vec{t} = (t_r, t_\theta, t_z)$  is the unit vector tangent to the interface, while  $P_0$ ,  $T$ ,  $R_1$ ,  $R_2$  represent the gas pressure, melt surface tension coefficient, the principal radius of curvature of the interface, and the radius of gas penetration region, respectively.

Substituting the stress tensor represented by the melt constitutive equation into the above two equations gives Eqs. (8b) and (8c). The boundary conditions at the gas penetration interface are written as

$$(u - U)n_r + wn_z = 0 \quad (8a)$$

$$\frac{\partial u}{\partial r} t_r n_r + \frac{1}{2} \left( \frac{\partial u}{\partial z} + \frac{\partial w}{\partial r} \right) (t_r n_z + t_z n_r) + \frac{\partial w}{\partial z} t_z n_z = 0 \quad (8b)$$

$$P - 2\eta \left[ \frac{\partial u}{\partial r} n_r^2 + \left( \frac{\partial u}{\partial z} + \frac{\partial w}{\partial r} \right) n_r n_z + \frac{\partial w}{\partial z} n_z^2 \right] = P_0 - \lambda \left( \frac{1}{R_1} + \frac{1}{R_2} \right) \quad (8c)$$

**2.2.2 Outer Solution.** An outer coordinate system for the gas-melt interface is set up as shown in Fig. 3(a). The governing equations and boundary conditions are transformed to be dimensionless.

$$\hat{r} = \frac{r-R}{b}, \quad \hat{z} = \frac{z}{b}, \quad \hat{h} = \frac{h}{b}, \quad \hat{u} = \frac{u-U}{U}, \quad \hat{w} = \frac{w}{U}, \quad \hat{P} = \frac{P-P_0}{b/T} \quad (9)$$

where  $R$  is the radius of gas core.

Based on the dimensionless variables, the governing equations and the boundary conditions could be transformed as

$$\frac{\partial u}{\partial r} + \frac{\delta}{1+\delta r} (u+1) + \frac{\partial w}{\partial z} = 0 \quad (10a)$$

$$\frac{\partial P}{\partial r} = \text{Ca} \left[ \frac{\partial^2 u}{\partial r^2} + \frac{\delta}{1+\delta r} \frac{\partial u}{\partial r} + \frac{\partial^2 u}{\partial z^2} - \frac{\delta^2}{(1+\delta r)^2} (u+1) \right] \quad (10b)$$

$$\frac{\partial P}{\partial z} = \text{Ca} \left[ \frac{\partial^2 w}{\partial r^2} + \frac{\delta}{1+\delta r} \frac{\partial w}{\partial r} + \frac{\partial^2 w}{\partial z^2} \right] \quad (10c)$$

$$\frac{dh}{dr} u - w = 0 \quad (11a)$$

$$\left[ 1 - \left( \frac{dh}{dr} \right)^2 \right] \left( \frac{\partial u}{\partial z} + \frac{\partial w}{\partial r} \right) - 2 \frac{dh}{dr} \left( -\frac{\partial u}{\partial r} + \frac{\partial w}{\partial z} \right) = 0 \quad (11b)$$

$$P - 2\text{Ca} \left[ \frac{\left( \frac{dh}{dr} \right)^2 \frac{\partial u}{\partial r} - \frac{dh}{dr} \left( \frac{\partial u}{\partial z} + \frac{\partial w}{\partial r} \right) + \frac{\partial w}{\partial z}}{1 + \left( \frac{dh}{dr} \right)^2} \right] = \frac{\frac{d^2 h}{dr^2}}{\left[ 1 + \left( \frac{dh}{dr} \right)^2 \right]^{3/2}} + \frac{\frac{dh}{dr}}{(1+\delta r) \left[ 1 + \left( \frac{dh}{dr} \right)^2 \right]^{1/2}} \quad (11c)$$

For convenience, the superscript ( ) of the variables is removed.

Supposing the gas penetration interface is  $z=h(r)$ , the following equation can be obtained

$$\frac{dz}{dr} = \frac{dh}{dr} = \frac{t_z}{t_r} = -\frac{n_r}{n_z} \quad (12)$$

Combining with boundary conditions, it follows that

$$P = -\text{Ca} \left[ 2 \frac{\partial u}{\partial r} + \frac{dh}{dr} \left( \frac{\partial u}{\partial z} + \frac{\partial w}{\partial r} \right) \right] + \frac{d^2 h}{dr^2} \left[ 1 + \left( \frac{dh}{dr} \right)^2 \right]^{-3/2} \quad (13)$$

By adopting  $\text{Ca}$  as perturbation parameter, examining the governing equations and boundary conditions when  $\text{Ca} \rightarrow 0$  with the perturbation theory, the approximation function of the  $h$  in the outer coordinate system can be obtained as

$$-1 = \frac{\frac{d^2 h^0}{dr^2}}{\left[ 1 + \left( \frac{dh^0}{dr} \right)^2 \right]^{3/2}} \quad (14)$$

Integrating the above equation by subjecting to the conditions

$$\frac{dh^0}{dr} = 0 \quad \text{at } r = -1 \quad \text{and} \quad h^0 = 0 \quad \text{at } r = 0$$

The outer solution is expressed as

$$h^0 = [1 - (r+1)^2]^{1/2} \quad (15)$$

**2.2.3 Inner Solution.** The point of intersection between the mold wall and the gas perturbation interface determined by the outer solution is the inconsistent region of the outer solution. This point is selected as the origin to set up the inner coordinate system. In this inner coordinate system, the variables are magnified  $\delta$  with  $\delta = \text{Ca}^m$ . To ensure that the magnified equations are in balance and is as simple as possible,  $m$  is preferred to be  $2/3$  [1] and

$$\bar{d} = \frac{1-\beta}{\text{Ca}^{2/3}}, \quad \bar{r} = \frac{r+1}{\text{Ca}^{2/3}}, \quad \bar{z} = \frac{z-1}{\text{Ca}^{2/3}}, \quad \bar{h} = \frac{h-1}{\text{Ca}^{2/3}}, \quad \bar{u} = u, \quad (16)$$

$$\bar{w} = \frac{w}{\text{Ca}^{1/3}}, \quad \bar{P} = P$$

Substituting the above equations into Eqs. (4) and (8), the resulting governing equations and boundary conditions in the inner coordinate system become

$$\frac{\partial \bar{u}}{\partial \bar{r}} + \frac{\partial \bar{w}}{\partial \bar{z}} = 0 \quad (17a)$$

$$\frac{\partial \bar{P}}{\partial \bar{r}} = \delta \frac{\partial^2 \bar{u}}{\partial \bar{r}^2} + \frac{\partial^2 \bar{u}}{\partial \bar{z}^2} \quad (17b)$$

$$\frac{\partial \bar{P}}{\partial \bar{z}} = \delta^2 \frac{\partial^2 \bar{w}}{\partial \bar{r}^2} + \delta \frac{\partial^2 \bar{w}}{\partial \bar{z}^2} \quad (17c)$$

$$\bar{w} = \frac{d\bar{h}}{d\bar{r}} \bar{u} \quad (18a)$$

$$\left( \frac{\partial \bar{u}}{\partial \bar{z}} + \delta \frac{\partial \bar{w}}{\partial \bar{r}} \right) \left[ 1 - \delta \left( \frac{d\bar{h}}{d\bar{r}} \right)^2 \right] - 4\delta \frac{\partial \bar{u}}{\partial \bar{r}} \frac{d\bar{h}}{d\bar{r}} = 0 \quad (18b)$$

$$\bar{P} = -2\delta \frac{\partial \bar{u}}{\partial \bar{r}} - \left( \delta \frac{\partial \bar{u}}{\partial \bar{z}} + \delta^2 \frac{\partial \bar{w}}{\partial \bar{r}} \right) \frac{d\bar{h}}{d\bar{r}} + \frac{d^2 \bar{h}}{d\bar{r}^2} \left( 1 + \delta \left( \frac{d\bar{h}}{d\bar{r}} \right)^2 \right)^{-(3/2)} \quad (18c)$$

Examining Eqs. (17) and (18) when  $\delta \rightarrow 0$  with the perturbation theory, the approximation function of  $\bar{h}$  in the inner coordinate system can be obtained as

$$\frac{\partial^3 \bar{h}}{\partial \bar{r}^3} = -\frac{3(\bar{h} + \bar{d})}{\bar{h}^3} \quad (19)$$

Employing fourth-order Runge–Kutta method to solve Eq. (19), the inner solution is as follows.

$$\bar{h}^0(\bar{x}) \approx \frac{A_2 \times 3^{2/3}(\bar{r} + \bar{r}_0)^2}{\bar{d}} + A_1 \times 3^{1/3}(\bar{r} + \bar{r}_0) + A_0 \times \bar{d} + O\left(\frac{1}{\bar{x}}\right) \quad (20)$$

where  $A_2 = -0.3215$ ,  $A_1 = -0.096$ , and  $A_0 = -2.9$ .

**2.2.4 Matching.** According to the matching asymptotic expansion theory, the inner solution at  $\bar{r} \rightarrow \infty$  matches the outer solution at  $r \rightarrow 1$ . This match is satisfied in any coordinate system, and herein the outer coordinate system is selected. Inverse transformation to the inner solution according to Eq. (16) results in

$$h^0(r) \approx 1 + \frac{A_2 \times 3^{2/3}(r+1)^2}{\bar{d}} + \dots \quad (21)$$

and when  $\hat{r} \rightarrow 1$ , the outer solution is

$$h^0(r) \approx 1 - (r+1)^2 + \dots \quad (22)$$

As  $(r+1)^n$  series are linear independent of each other, the coefficients of  $(r+1)^n$  of the two solutions should be equivalent. Therefore,  $\bar{d}$  could be obtained as

$$\bar{d} = -2A_2 \times 3^{2/3} = 1.3375 \quad (23)$$

Consequently, the gas penetration thickness ratio in the steady penetration region is calculated by

$$\beta = 1 - \delta \bar{d} = 1 - 1.3375Ca^{2/3} \quad (24)$$

**2.2.5 Correction.** Equation (24) is the calculating model for deducing gas penetration thickness ratio. This calculation will lead to serious deviation when  $Ca$  becomes larger. A correction is needed to make the model applicable to a large range of  $Ca$ .

The correction function of gas penetration in the outer coordinate system is expressed by

$$h(r) \approx \beta - De^{\mu r} \quad (25)$$

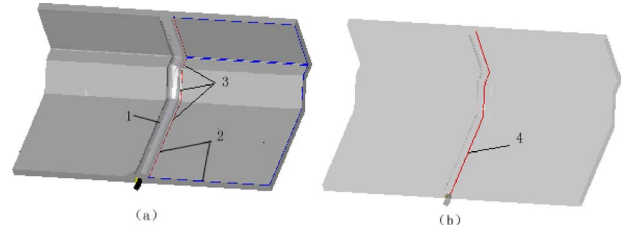


**Fig. 4 Involved concepts for gas-channel mesh: (1) gas channel, (2) surface boundary, (3) path of gas channel, and (4) center line of gas channel**

where  $D$  and  $\mu$  are constants needed to be obtained.

According to the no-slip condition at the mold wall, the velocity and pressure can be defined by

$$u(r, z) \approx -1 + e^{\mu r} \xi_1(z) + o(e^{2\mu r}) \quad (26a)$$

$$w(r, z) \approx e^{\mu r} \xi_2(z) + o(e^{2\mu r}) \quad (26b)$$

$$P(r, z) \approx Ca e^{\mu r} \xi_3(z) + o(e^{2\mu r}) \quad (26c)$$

where  $\xi_1$ ,  $\xi_2$ , and  $\xi_3$  are functions to be solved.

By applying Eqs. (25) and (26) to the governing and boundary condition equations and by expressing  $\xi_2$  by a trigonometric function serious expansion, the simultaneous equations with respect to all educible constants can be obtained, and these constants will be calculated by solving these equations.

During the penetration process, at each increment time step, the gas penetration thickness ratio is calculated by Eq. (24), and then corrected by Eq. (25). Because the governing and boundary condition equations at each penetration position have been taken into account in the correction, it will lead closer to approximation in a large range of  $Ca$ .

### 3 Implementation

**3.1 Gas-Channel Mesh Generation.** After generating triangular elements on the surface model based on the Delaunary triangulation method, an approach of generating the gas-channel mesh semiautomatically was put forward by combing the manual selection of the gas-channel path and the automatic calculation of the channel nodal parameters.

The path of the gas channel was selected manually. For the sake of conduit for gas penetration, GAIM products are generally designed with some thicker structures, such as ribs and bosses, to be gas channels. The region of the gas channel in the GAIM product could be determined. On the basis of the surface mold, which consists of a certain amount of triangle elements, identifying the gas channel and obtaining some lines by open manual operation were feasible. These lines were named surface boundary in the following. Once the direction of surface boundary was identical or approximately identical to that of the path of the gas channel, surface boundary could be selected as the path of the gas channel, as shown in Fig. 4.

Since selecting the path of the gas channel manually was equivalent to finding the thicker parts in the GAIM products, and the gas penetrated toward the thickest positions of thicker parts, it was necessary to calculate the parameter of the gas-channel node automatically. Due to the surface tension of viscid liquid, the cross section of the gas core after gas penetration is usually inclined to circularity. The center of maximum inscribed circle of cross section of the gas core was considered as the thickest position as well as the location where gas penetrated with the highest probability. In order to define the geometry model of gas-channel mesh, it was assumed that the gas mesh comprises an array of gas-channel nodes with topologic relationship among them. Two adjacent gas-channel nodes constituted a gas-channel element as shown in Fig. 5. According to the above expatiate, the coordinates of a gas-

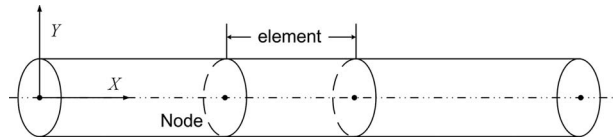


Fig. 5 Schematic notation for gas-channel mesh

channel node was equal to that of the center of maximum inscribed circle of the cross section of the gas core, and the radius of a gas-channel node was also calculated as the equivalent radius of the cross section of the gas core, which is  $R_{eq} = \sqrt{A/\pi}$ , where  $R_{eq}$  is the equivalent radius and  $A$  is the area of cross section of the gas channel. After constructing the topologic relationship of the gas-channel nodes, the gas-channel mesh was generated.

The procedure of the gas-channel mesh generation was summarized as follows.

- Step 1. Import GAIM product and use the Delaunary triangulation method to generate surface model.
- Step 2. Identify the gas-channel region of GAIM product artificially.
- Step 3. Generate surface boundary based on the surface model by open operation and selecting surface boundary to ascertain the path of gas channel manually.
- Step 4. Calculate the location and the radius of the gas nodes based on the path of the gas channel.
- Step 5. Build the topology of gas mesh.

**3.2 Numerical Solution.** Based on the previously described Eq. (2) and introducing appropriate boundary conditions, we could infer the following melt-filling pressure equation:

$$\nabla \cdot (S \nabla P) = 0 \quad (27)$$

where  $S$  was calculated by

$$S = \int_0^b \frac{(b-z)^2}{\eta} dz \quad (28)$$

where  $b$ ,  $z$ , and  $\eta$  represent half-gapwise thickness, gapwise direction, and melt viscosity, respectively. Applying the Galerkin method, the pressure finite element was deduced as

$$\sum_l S^{(l)} \sum_{j=1}^3 D_{ij}^{(l)} P_{N'} = 0 \quad (29)$$

where  $l$  traversed all elements, which included nodes  $N$ ,  $i$ , and  $j$  as the local number in element  $l$  corresponding to the node numbers  $N$  and  $N'$  in whole, respectively. The  $D_{ij}^{(l)}$  was defined as

$$D_{ij}^{(l)} = \int_{A^{(l)}} [\nabla L_i^{(l)}(x,y) \cdot \nabla L_j^{(l)}(x,y)] dA \quad (30)$$

where  $A^{(l)}$  represented a triangular finite element and  $L_i^{(l)}$  was the pressure trial function in the finite element.

GAIM filling process includes melt flow and gas penetration. For melt flow, a hybrid CV/FEM/FDM was employed in the gas-assisted injection molding filling simulation, and a standard finite-difference technique was used to discretize the timewise and gapwise (thickness) coordinates. First, the boundary conditions were initialized, and the pressure field was initialized according to the injection process settings followed by calculating the melt viscosity and pressure system matrix. By solving the pressural finite element (Eq. (29)), pressure distribution could be obtained. In terms of the pressure distribution, the flux of each node was calculated; in the meantime, the melt flow front advancement was realized. Then the energy equation was applied to all elements and nodes, and the nodal temperature at each layer in the gapwise

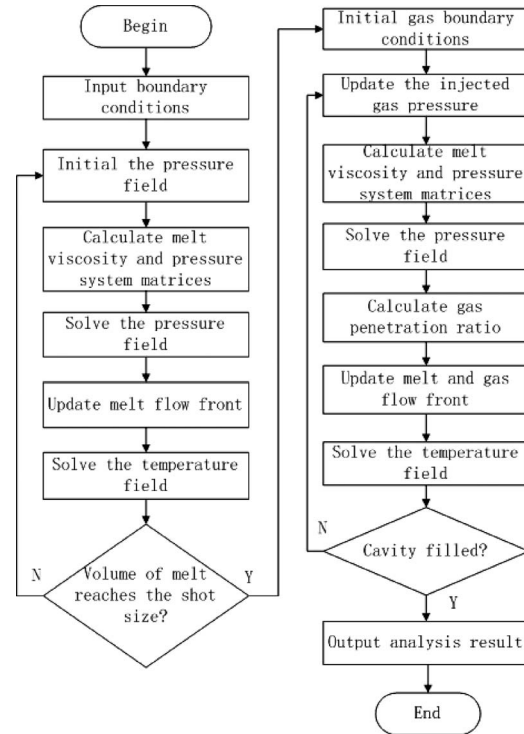


Fig. 6 Flow chart for numerical implement of GAIM

direction was calculated. The above process was repeated until the volume of melt arrived at the shot size as shown in Fig. 6.

At the gas injection stage, the governing equations of melt flow could be solved by the methods mentioned above. With respect to the gas penetration process, the key points were calculating the gas penetration radius and the gas front advancement. In terms of the geometry relationship between gas-channel nodes and surface nodes and the filling order of surface nodes, the topology relationship between gas-channel nodes and surface nodes was built. According to Eq. (24), the gas penetration thickness was only the function of the capillary number  $Ca$ , where  $\eta$  and  $U$  were the viscosity and velocity of melt at the gas/melt interface, respectively, whereas  $\lambda$  was the melt surface tension coefficient. With the Cross viscosity model,  $\eta$  was obtained according to the distribution of pressure, temperature, and shear rate of melt at the gas/melt interface;  $U$  was calculated according to the momentum formulation and pressure gradient at the gas penetration front; and  $\lambda$  could be acquired by literatures for different materials. Therefore, the gas penetration ratio at the gas/melt interface could be calculated.

For the gas penetration front advancement, the control-volume method was employed. Gas-channel elements were subdivided into halves. The control volume associated with a node was defined as the union of all subdivided volumes that were concerned to that node as shown in Fig. 7. During the gas penetration process, the gas-channel mesh was divided into five regions: control volume not filled by melt and injected gas,  $f_{melt}=0$ ,  $f_{gas}=0$ ; control volume already filled by melt but not with completeness and

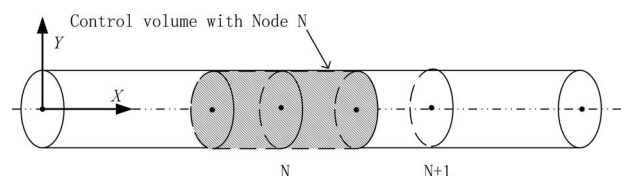
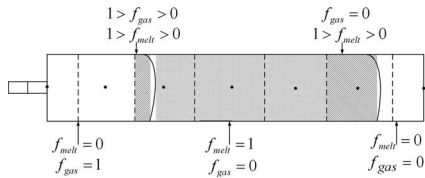


Fig. 7 Schematic notation for control volume of gas node



**Fig. 8 Schematic notation for filling status in gas-channel mesh**

not filled by gas, i.e., melt front,  $1 > f_{melt} > 0$ ,  $f_{gas} = 0$ ; control volume filled by melt completely but not filled by gas,  $f_{melt} = 1$ ,  $f_{gas} = 0$ ; control volume already penetrated by gas but not with completeness, which is the gas penetration front,  $1 > f_{melt} > 0$ ,  $1 > f_{gas} > 0$ ; and control volume penetrated by gas completely,  $f_{melt} = 0$ ,  $f_{gas} = 1$  (as shown in Fig. 8).

In terms of the pressure distribution, the melt flux rate flowing into control volume at the melt flow front and the gas flux rate penetrating into control volume of gas penetration front were ob-

tained. If the time increment was set as the time, which completely filled the control volume of only one node at the melt flow front or at the gas penetration front, the computation time should be very long. In order to shorten the computation time, the filling time of control volume of only one node at the gas penetration front was set as the time increment, considering that the number of gas-channel nodes was much smaller than that of nodes of surface model. After the melt flow front and the gas penetration front were updated, the filling status of each gas-channel node could be obtained.

#### 4 Verification

HSCAE (Huasu CAE), developed by the authors based on the model presented, is a simulation system for injection molding similar to MOLDFLOW MPI. Figure 9 displays the geometry of the experimental part whose size is  $225.9 \times 74.9 \times 37.1 \text{ mm}^3$ . The beams in Fig. 10(a) and the little bars signed with "A" in Fig. 11(a) are the runner systems, and the little bars signed with "A" in Fig. 10(a) and Fig. 11(a) denote the gas pin location. The posi-



**Fig. 9 The geometry of the experimental test part**

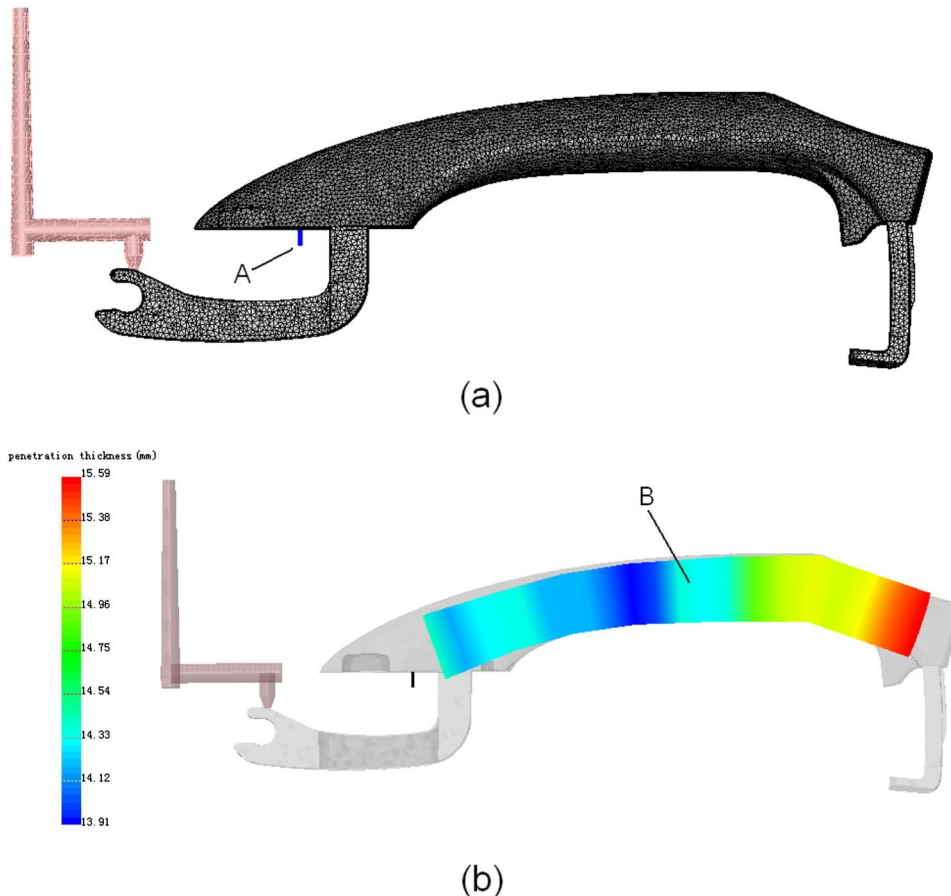


**Fig. 10 The simulation by HSCAE: (a) the surface model composed of triangle element and (b) the penetration thickness**

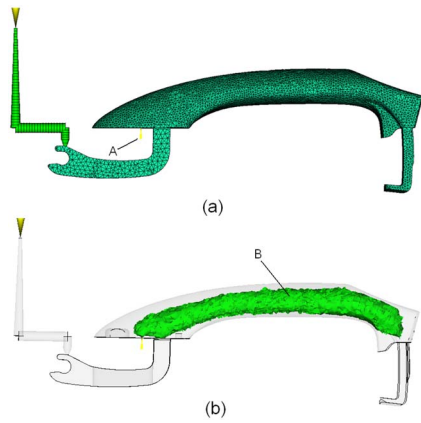


**Fig. 11** The simulation by MOLDFLOW: (a) the tetrahedral finite element and (b) the penetration thickness

tions signed with 1, 2, 3, 4, 5, and 6 are the gas penetration thickness measured positions. The selected material is PA6, namely, Ultramid B3EG6. The major processing conditions are a shot size of 71.1%, a delay time of 4.0 s, a mold surface temperature of 60.0 °C, a melt temperature of 280.0 °C, and a pressure-control gas injection with initial pressure of 4.0 MPa and degressive speed of 0.2 MPa/s. Figures 10 and 11 show the mesh and gas penetration thickness simulated by HSCAE and MOLDFLOW, respec-

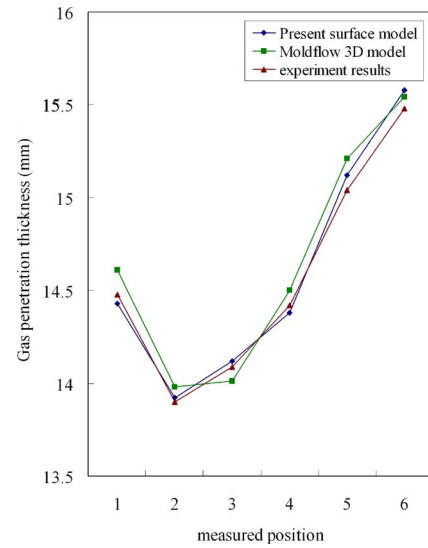


**Fig. 12** The comparison between experimental result and the corresponding results of simulation by MOLDFLOW and HSCAE

tively, in corresponding conditions. The regions signed with “B” in Fig. 10(b) and in Fig. 11(b) denote the gas core. The number of part elements in HSCAE is 47,268 and 14,6473 in MOLDFLOW. Although the number in HSCAE is much less than that in MOLDFLOW,

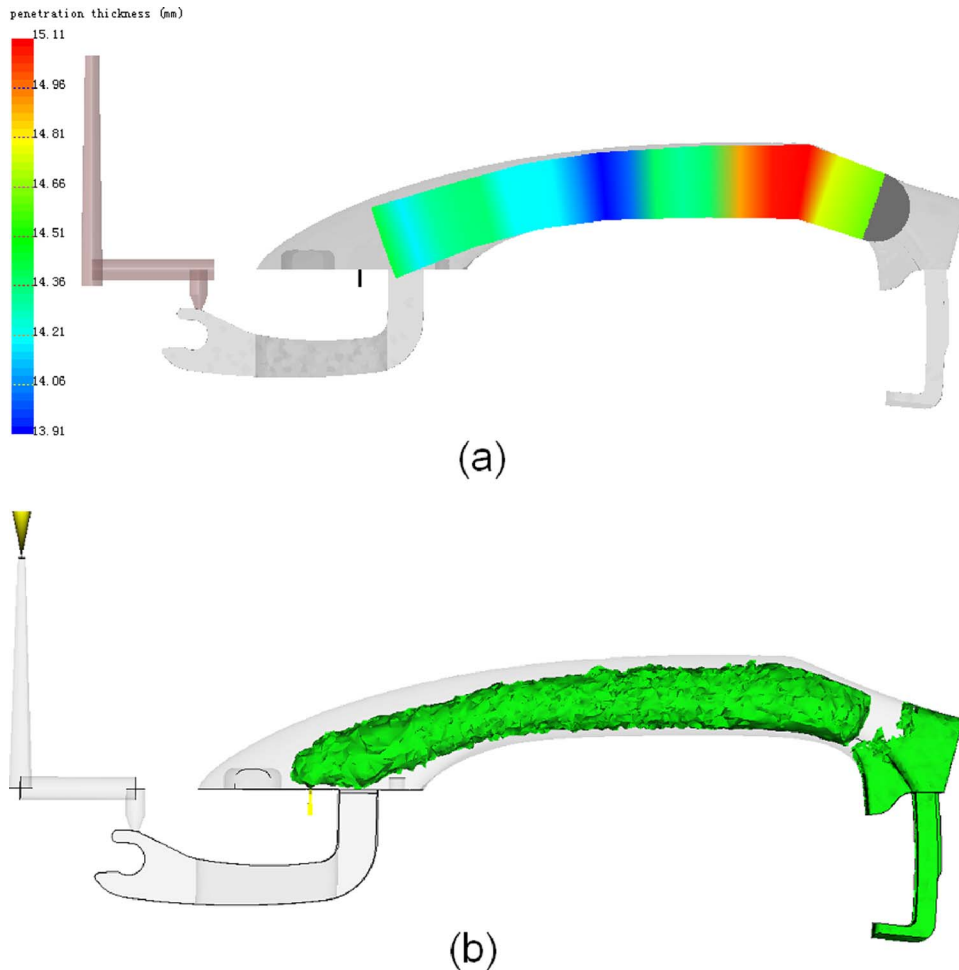


**Fig. 13** The simulated penetration thickness under new processing settings by (a) HSCAE and (b) MOLDFLOW

the mesh in HSCAE is much refined since 3D mesh is used in MOLDFLOW. The employed configuration in simulation is 2.4Gbyte CPU and 1Gbyte RAM. The processing time is 21 mins in HSCAE and 96 mins in MOLDFLOW. It is obvious that the processing time in HSCAE is much shorter. After demolding, the molded part is dissected and photographed and the skin melt thickness is measured (skin melt thickness ratio  $\gamma=1-\beta$ ), with a maximum variation of 0.1 mm. The predicted results by HSCAE and MOLDFLOW as well as experiment in the penetration thickness measured points are plotted in Fig. 12 for comparison. It can be seen that the predicted results based on the proposed model agree well with the results simulated by MOLDFLOW, with the maximum relative deviation being 6.5%.

Another numerical experiment using different process settings for the same part is presented as follows. The shot size of melt is reduced from 71.1% to 60.0% and the other processing conditions are the same as those of the previous one. As we all know, the reduction in the shot size of melt leads to the occurrence of the gas blow out. The simulation results of HSCAE and MOLDFLOW are both shown in Fig. 13. As shown in Fig. 13(a), HSCAE predicts the occurrence of blow out of gas accurately, the gray hemisphere at the right hand of the gas core denotes the location of a gas blow out. On the other hand, the gas is injected into the melt just from one gas pin in the added simulation, therefore the gas core region must be interconnected, no matter if the blow out of gas takes place. But in the result of MOLDFLOW, as shown in Fig. 13(b), the phenomenon of the gas blow out cannot be found and the simulated gas core region is not interconnected at all. This means that when the gas blow out takes place, MOLDFLOW gives an obviously unreasonable result. This added simulation demonstrates that the proposed method can work on a wider range than MOLDFLOW.

## 5 Conclusions

A GAIM filling process model, based on the surface model and the theory model of gas-assisted displacement of viscous fluid, was presented, and the technology of generating the gas-channel mesh semiautomatically is proposed. Due to the surface model adopted, efficiency and stability of calculation were assured compared with the 3D mesh. Furthermore, the problems of the second modeling of the midplane model and gas channel are avoided; hence the defects of the current packages as described in Sec. 2 have been solved. The comparison with the experiment and MOLDFLOW shows that the presented model and simulation is reliable. But it should be noted that the presented model has three limitations. First, it has an assumption: gas core is a circular section or almost circular section. This model would be not so effective when the section of the gas core is far from a circle. Second, the assumption of axisymmetry may be not valid when the gas changes its penetration direction dramatically, due to the fact that the gas always chooses the easiest path to flow and the path fol-

lowing the inner radius has the shortest length. Third, it does not take the gas secondary penetration into account. These limitations should be addressed in later study.

## Acknowledgment

The authors would like to acknowledge financial support from the National Natural Science Foundation Council of China (Grant No. 50675080) and Doctoral Fund of Ministry of Education of China (Grant No. 20060487056).

## References

- [1] Zhou, H. M., and Li, D. Q., 2003, "Filling Simulation and Gas Penetration Modeling for Gas-Assisted Injection Molding," *Appl. Math. Model.*, **27**(11), pp. 849–860.
- [2] Isayev, A. I., Shell, R. I., and Hall, E. L., 2000, *Molding Processes in Handbook of Industrial Automation*, Marcel Dekker, New York.
- [3] Avery, J., 2000, *Gas-Assist Injection Molding: Principal and Applications*, Hanser, Munich.
- [4] Haagh, G. A. A. V., Perters, G. W. M., Van De Vosse, F. N., and Meijer, H. E. H., 2001, "A 3-D Finite Model for Gas-Assisted Injection Mold: Simulations and Experiments," *Polym. Eng. Sci.*, **41**(3), pp. 449–465.
- [5] Li, C. T., Shin, J. W., and Isayev, A. I., 2004, "Primary and Secondary Gas Penetration During Gas Assisted Injection Molding. Part II: Simulation and Experiment," *Polym. Eng. Sci.*, **44**(5), pp. 992–1002.
- [6] Zhou, H. M., and Li, D. Q., 2001, "A Numerical Simulation of the Filling Stage in Injection Molding Based on Surface Model," *Adv. Polym. Technol.*, **20**(2), pp. 125–131.
- [7] Chiang, H. H., Hieber, C. A., and Wang, K. K., 1991, "A Unified Simulation of the Filling and Post Filling Stages in Injection Molding. Part I: Formulation," *Polym. Eng. Sci.*, **31**(2), pp. 116–124.
- [8] Yang, S. Y., and Liu, S. J., 1995, "Development of Mold Ability Diagrams for Gas-Assisted Injection Molding," *Adv. Polym. Technol.*, **14**(3), pp. 197–205.
- [9] Yang, S. Y., Huang, F. Z., and Liu, W. N., 1996, "A Study of Rib Geometry for Gas-Assisted Injection Molding," *Polym. Eng. Sci.*, **36**(23), pp. 2824–2831.
- [10] Huzyak, P. C., and Koelling, K. W., 1997, "Penetration of a Long Bubble Through a Viscoelastic Fluid in a Tube," *J. Non-Newtonian Fluid Mech.*, **71**(1–2), pp. 73–88.
- [11] Polynkin, A., Pittman, J. F. T., and Sienz, J., 2005, "Gas Assisted Injection Molding of a Handle: Three-Dimensional Simulation and Experimental Verification," *Polym. Eng. Sci.*, **45**(8), pp. 1049–1058.
- [12] Ilinca, F., and Hetu, J. F., 2006, "Numerical Investigation of the Flow Front Behavior in the Co-Injection Molding Process," *Int. J. Numer. Methods Fluids*, **50**(12), pp. 1445–1460.
- [13] Bretherton, F. P., 1961, "The Motion of Long Bubbles in Tubes," *J. Fluid Mech.*, **10**(2), pp. 166–188.
- [14] Reinelt, D. A., and Saffman, P. G., 1985, "Penetration of a Finger Into a Viscous Fluid in a Channel and Tubes," *SIAM (Soc. Ind. Appl. Math.) J. Sci. Stat. Comput.*, **6**(3), pp. 542–561.
- [15] Kolb, W. B., and Cerro, R. L., 1991, "Coating the Inside of a Capillary of Square Cross Section," *Chem. Eng. Sci.*, **46**(9), pp. 2181–2195.
- [16] Belblidia, F., Pittman, J. F. T., Polynkin, A., and Sienz, J., 2005, "Gas Displacing Viscous Shear Thinning Liquids From Tubes: Effects of Cooling Before Gas Injection," *Chem. Eng. Sci.*, **60**(17), pp. 4953–4956.
- [17] Shen, Y. K., 2001, "The Study on Polymer Melt Front, Gas Front, and Solid Layer in Filling Stage of Gas-Assisted Injection Molding," *Int. Commun. Heat Mass Transfer*, **28**(1), pp. 139–148.
- [18] Chen, S. C., Hu, S. Y., and Chao, S. M., 2000, "Simulation of a Mold-Cooling Process for Gas-Assisted Injection Molded Parts Designed With a Top Rib on the Gas Channel," *Polym. Eng. Sci.*, **40**(3), pp. 595–606.